frontiers in Built Environment

TYPE Original Research
PUBLISHED 10 April 2026
DOI 10.3389/fbuil.2026.1745681

OPEN ACCESS

EDITED BY
Emilio Bilotta,
University of Naples Federico II, Italy

REVIEWED BY
Tony Fierro,
University of Molise, Italy
Lucia Mele,
University of Naples Federico II, Italy

*CORRESPONDENCE
Michael A. Hicks,
m.a.hicks@tudelft.nl

RECEIVED 13 November 2025
REVISED 21 January 2026
ACCEPTED 02 February 2026
PUBLISHED 10 April 2026

CITATION
González Acosta JL, van den Eijnden AP and Hicks MA (2026) Application of the random finite element method to assess traditional techniques used to analyse free-field ground response and liquefaction triggering.
Front. Built Environ. 12:1745681.
doi: 10.3389/fbuil.2026.1745681

Application of the random finite element method to assess traditional techniques used to analyse free-field ground response and liquefaction triggering

J. León González Acosta[1,2], Abraham P. van den Eijnden[2,3] and Michael A. Hicks[2]*

[1]Geoscience and Technology, Energy and Materials Transition, TNO Utrecht, Netherlands, [2]Section of Geo-Engineering, Faculty of Civil Engineering and Geosciences, Delft University of Technology, Delft, Netherlands, [3]Safe and Resilient Infrastructure, Deltares, Delft, Netherlands

Traditional one-dimensional (1D) techniques for analysing free-field ground response and liquefaction triggering rely on the assumption of ideal, homogeneous soil deposits, which are hardly ever encountered. This paper highlights the inaccuracies and limitations of 1D schemes and the motivation for two-dimensional (2D) strategies using the random finite element method (RFEM). Through Monte Carlo simulations, the 2D dynamic response of various soil domains, considering the impact of spatial variability of void ratio on liquefaction potential, is analysed. Each 2D realisation has been re-examined by splitting the domain into 1D soil columns while preserving similar variability attributes. The results reveal significant differences. While 2D schemes show a reduced variability in the ground surface responses and more realistic liquefaction spreading compared to 1D simulations, 2D schemes indicate more severe impacts on ground surface accelerations, response spectra peak values, and energy released. For site response analysis using a homogeneous soil profile, a characteristic void ratio value based on the mean minus 2 standard deviations is suitable for high PGA potential scenarios. However, the differences in responses between 1D and 2D schemes diminish if the input earthquake acceleration is not strong enough to cause liquefaction.

KEYWORDS
coupled random finite element method, earthquake, hypoplasticity, liquefaction, Monte Carlo simulations, random fields, site response analysis

1 Introduction

Understanding free-field ground response due to seismic activity is an essential requirement in geotechnical engineering for design purposes and analysing soil-structure interaction problems. Much research has been conducted to study the different aspects affecting free-field ground response, with one of the most important of these being the potential for soil liquefaction. During the late 1960s and early 1970s, some of the most influential work describing liquefaction was conducted (Seed and Lee, 1966; Lee and Seed, 1967; Seed and Idriss, 1967; Seed and Idriss, 1971; Shibata et al., 1972). Subsequently, liquefaction principles were combined with standard finite element (FE) procedures to

analyse free-field ground response within a numerical framework (Ghaboussi and Dikmen, 1977; Prevost, 1986). More recently, a large number of studies analysing the geotechnical seismic behaviour of complex structures have been reported (Koutsourelakis et al., 2002; Chian et al., 2014; Sumer, 2014; Vargas-Moreno et al., 2016; Luque and Bray, 2020). However, although substantial attempts have been made to provide an accurate description of ground behaviour and liquefaction development during earthquakes, most investigations have disregarded the horizontal effects due to soil spatial variability, a simplification that can cause significant divergence of results (Maharjan and Takahashi, 2013; Pretell et al., 2022).

It is common practice in earthquake engineering for free-field ground response analyses to be performed through one- and two-dimensional soil models considering idealised soil deposits (e.g., in 1D models, perfectly horizontal layered and homogeneous). This simplified soil domain representation is common since underground data are not always available. Besides, simulating material variability using recognised geomechanical software is complicated or not possible. To overcome this limitation, some authors began implementing standard techniques of random field theory in the study of site seismic analysis (e.g., Popescu et al., 1995; Fenton and Vanmarcke, 1998). Currently, there are two common strategies in the study of soil behaviour in combination with random field theory, the first being based on the random finite element method (RFEM) (Griffiths and Fenton, 2004). RFEM combines finite element (FE) analysis with random field theory, and, through Monte Carlo simulations, realistic predictions of soil liquefaction and free-field ground response can be obtained during earthquake simulations (Popescu et al., 1997; Assimaki et al., 2003; Popescu et al., 2005; Montgomery and Boulanger, 2016). In contrast, the second strategy does not simulate the earthquake; rather, the liquefaction potential and/or ground behaviour are estimated via CPT and/or SPT correlations in which the soil domain is simulated using random field methods (Chen et al., 2016; Stuedlein and Bong, 2017; Wang et al., 2017; Bong and Stuedlein, 2018). In essence, the former strategy provides a fully coupled stochastic–dynamic analysis based on finite-element simulations that explicitly accounts for soil constitutive behaviour, whereas the latter offers a probabilistic but simplified assessment based on empirical triggering relationships, without explicit finite-element modelling or constitutive formulations. Results obtained by applying each strategy show significant differences with results obtained by traditional (deterministic) techniques. Nevertheless, despite both strategies showing advantages over traditional schemes, the first one is often preferred due to the incorporation of an actual earthquake and soil constitutive behaviour, hence guaranteeing feasible geo-structural responses (Basu et al., 2019a).

Unfortunately, regardless of its advantages, the first strategy is computationally costly, due to the need to simulate material constitutive behaviour in a dynamic context, and this has limited its potential for practical application. Most existing work using RFEM has focused on the analysis of specific historical cases, and conclusions are based on a limited number of simulations. Furthermore, the limitations of one-dimensional models are still not properly reported. Attempts to demonstrate the limitations of traditional techniques have been made (Basu et al., 2019b; González Acosta et al., 2022a), but analyses have considered the behaviour of an individual or only relatively few scenarios. In this paper, the limitations and inaccuracies of traditional 1D soil column schemes to analyse free-field ground behaviour and liquefaction development are investigated via RFEM. The correlation between independent 1D columns and 2D simulations is guaranteed by constructing 1D columns using the same randomly distributed material properties as for the 2D domains, where the void ratio e is the randomised parameter. The results are presented in terms of probability density functions (pdf's) and cumulative distribution functions of physical, ground-motion intensity, and energy-related indicative values. Regarding physical measurements, the liquefaction area (A_L) in time is studied. In terms of ground-motion intensity and energy-related indicators, the peak ground acceleration (PGA), Arias intensity (I_a), and response spectrum function (RSF) are considered. First, the theoretical background of random fields is presented. Then, a brief description of the coupled finite element method (FEM) and small-strain hypoplastic model theory are given. The benchmark used to study the limitations of 1D schemes is next introduced and comparative remarks based on the obtained results are presented, indicating the most significant differences between one- and two-dimensional schemes. Finally, a parametric study is included to give guidance on the most reliable set of parameters needed to obtain similar results between 1D and 2D simulations. Note that this paper considers only a single earthquake acceleration and the spatial variability of only void ratio to maintain simplicity and to yield demonstrative insights, considering that the inclusion of multiple earthquake input motions and spatially variable parameters would result in complex scenarios, making it difficult to isolate the effects of the earthquake motion and the soil properties. The results should therefore be considered as preliminary, and only indicative of the possible repercussions of soil spatial variability in the study of liquefaction triggering. A more comprehensive study incorporating more than one earthquake acceleration and the spatial variability of more than one soil parameter is outside the current scope, but is seen as necessary future work.

2 Random fields and coupled-cyclic FEM theoretical background

2.1 Random fields

Random field methods are numerical techniques for distributing parameter values spatially over a domain. Various procedures have been developed, such as local average subdivision (LAS) (Fenton and Vanmarcke, 1990), covariance matrix decomposition (CMD) (Fenton and Griffiths, 2008), sequential Gaussian methods (Deutsch and Journel, 1992), and variants of linear estimation (Liu et al., 2004; Xiao et al., 2016). Among these techniques, LAS has been shown to be suitable for analysing numerous geotechnical problems, including liquefaction triggering (Hicks and Onisiphorou, 2005). LAS constructs random fields of material properties through (i) a probability density function, described by a mean μ and standard deviation σ (in which $V = \sigma/\mu$ is the coefficient of variation), and (ii) a spatial correlation function, defined by horizontal and vertical scales of fluctuation, θ_H and θ_V, respectively, representing the distances over which property values are significantly correlated. Figure 1a shows an illustrative sketch of a void ratio, e, distribution with depth, while Figure 1b shows the probability density function of e.

10.3389/fbuil.2026.1745681

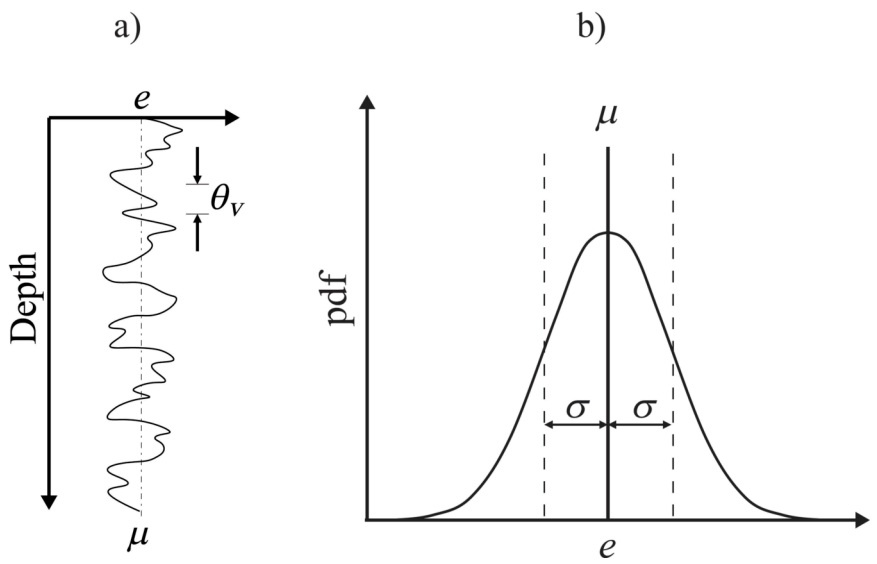

FIGURE 1
(a) Variation of void ratio *e* with depth, and **(b)** probability density function of *e*, after Hicks and Samy (2002).

Various functions can be selected to obtain the spatial correlation between two points. Herein, the spatial correlation function is given by Equation 1:

$$\rho_{spatial}(\tau) = \exp(-2\tau);\ \tau = \sqrt{\left(\frac{\Delta x_1}{\theta_H}\right)^2 + \left(\frac{\Delta x_2}{\theta_V}\right)^2} \tag{1}$$

where ρ_{spatial} $(\bullet)$ is the spatial correlation function, τ is the normalised distance with respect to the scales of fluctuation, θ_H and θ_V, and $\vec{x}$ are the spatial coordinates. This function is selected as it provides an efficient and realistic representation of the spatial correlation of soil properties (Varkey et al., 2023).

To determine the range and relative likelihood of solutions to a given problem, a Monte Carlo simulation is required, in which multiple realisations of the spatial variability are generated based on the same input statistics (μ, σ, and θ) in order that a distribution of possible model outcomes can be computed via FEM.

2.2 Coupled-cyclic FEM

In this section, a brief introduction to the governing equations, discretisations and constitutive behaviour for the saturated soil material are presented considering a so-called *u-p* formulation. For a detailed elaboration of the governing equation discretisations the reader is directed to Zienkiewicz et al. (1999), and for a description of the constitutive behaviour the reader is directed to Niemunis and Herle (1997) and Gudehus et al. (2008). The coupled-cyclic FEM has been assembled using an in-house FORTRAN architecture based on the building-block philosophy of Smith et al. (2013), whereby the finite-element solver is structured into modular components for mesh generation, numerical integration, global matrix assembly, boundary condition enforcement, and solving of the system of equations.

2.2.1 Governing equations

For a fully saturated porous medium, the momentum balance and mass conservation equations are

$$\mathbf{B}^{\mathrm{T}}\boldsymbol{\sigma} - \rho\ddot{\mathbf{u}} + \rho\mathbf{b} = \mathbf{0} \tag{2}$$

$$\nabla^{\mathrm{T}}\left(k\left(-\nabla p_{\mathrm{w}} + \rho_{\mathrm{w}}\mathbf{b}\right)\right) + \alpha\mathbf{m}\mathbf{B}\dot{\mathbf{u}} + \frac{\dot{p}_{\mathrm{w}}}{Q} = \mathbf{0} \tag{3}$$

where $\mathbf{B}$ is the strain–displacement matrix, $\boldsymbol{\sigma}$ is the stress tensor, $\mathbf{u}$ is the vector of nodal displacements, $\mathbf{b}$ is the body force, ρ is the mixture density ($\rho = n\rho_{\mathrm{w}} + (1 - n)\rho_{\mathrm{s}}$, in which n is the porosity, ρ_{w} is the water density, and ρ_{s} is the soil particle density), k is the soil isotropic permeability, and Q is defined as $1/Q = n/K_{\mathrm{w}} + (1 - n)/K_{\mathrm{s}}$, in which K_{w} and K_{s} are the bulk moduli of the water phase and soil particles, respectively. Meanwhile, the incremental effective stress–strain relationship may be given by Equations 4 and 5:

$$\mathrm{d}\boldsymbol{\sigma}' = \mathrm{d}\boldsymbol{\sigma} - \alpha\mathbf{m}p_{\mathrm{w}} \tag{4}$$

$$\mathrm{d}\boldsymbol{\sigma}' = \mathbf{D}\mathrm{d}\boldsymbol{\varepsilon} \tag{5}$$

where $\mathrm{d}\boldsymbol{\sigma}'$ and $\mathrm{d}\boldsymbol{\sigma}$ are the incremental effective and total stresses, respectively, α is a constant usually considered as $\alpha = 1$ for soils, p_{w} is the pore water pressure, $\mathbf{m}^{\mathrm{T}} = \{1\ 1\ 0\ 1\}$, $\mathbf{D}$ is the tangent matrix dependent on the state variables and history, and $\mathrm{d}\boldsymbol{\varepsilon}$ is the strain increment vector.

2.2.2 Space and time discretisations

The weak form of the governing equations (Equations 2, 3) is written in matrix notation as Equation 6:

$$\begin{bmatrix} \tilde{\mathbf{M}} & \mathbf{0} \\ \mathbf{0} & \mathbf{0} \end{bmatrix} \begin{Bmatrix} \ddot{\tilde{\mathbf{u}}} \\ \ddot{\tilde{\mathbf{p}}} \end{Bmatrix} + \begin{bmatrix} \tilde{\mathbf{C}} & \mathbf{0} \\ \tilde{\mathbf{Q}}^{\mathrm{T}} & \mathbf{S} \end{bmatrix} \begin{Bmatrix} \dot{\tilde{\mathbf{u}}} \\ \dot{\tilde{\mathbf{p}}} \end{Bmatrix} + \begin{bmatrix} \tilde{\mathbf{K}} & -\tilde{\mathbf{Q}} \\ \mathbf{0} & \mathbf{H} \end{bmatrix} \begin{Bmatrix} \tilde{\mathbf{u}} \\ \tilde{\mathbf{p}} \end{Bmatrix} = \begin{Bmatrix} \tilde{\mathbf{f}}_{\mathrm{s}} \\ \tilde{\mathbf{f}}_{\mathrm{w}} \end{Bmatrix} \tag{6}$$

where $\tilde{\mathbf{M}}$ is the mass matrix, $\tilde{\mathbf{Q}}$ is a matrix describing the hydro-mechanical coupling between the soil skeleton deformation and the

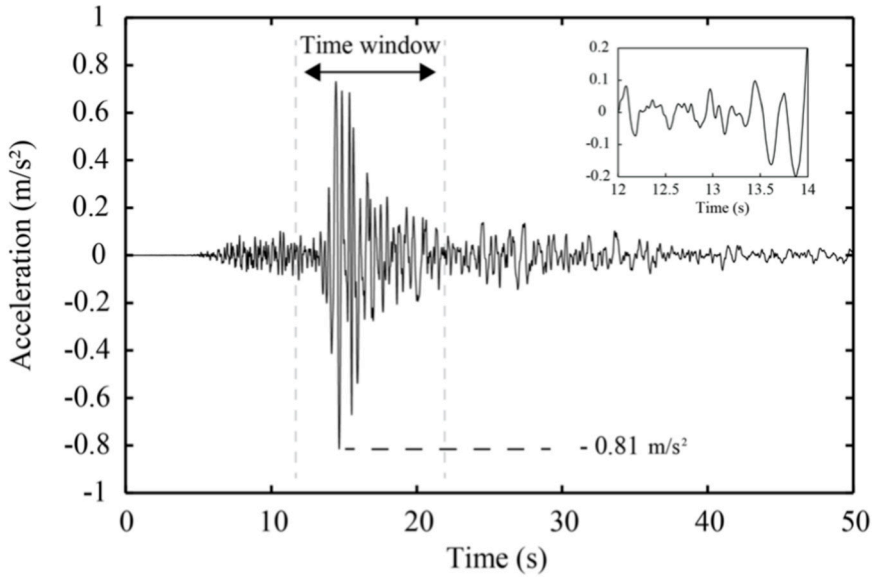

FIGURE 2
1999 Chi-Chi recorded accelerogram (component 90, station CWB HWA039 recorded at 48.1 km from the hypocentre) and simulation window. Acceleration data modified from the California Geological Survey and U.S. Geological Survey (2005).

TABLE 1 Soil parameters [after Herle and Gudehus (1999)].

ϕ_c	p_t	h_s	n	e_{d0}	e_{c0}	e_{i0}	α	β	m_R	m_T	R	β_r	χ
(°)	(kPa)	(kPa)	-	-	-	-	-	-	-	-	-	-	-
33	$1.0E^{-5}$	$1.5E^{6}$	0.28	0.55	0.95	1.05	0.25	1.5	5.0	2.0	$1.0E^{-4}$	0.5	6

pore water flow, **S** and **H** are the compressibility and permeability matrices of the pore fluid, $\tilde{\mathbf{K}}$ is the stiffness matrix of the drained behaviour defined in terms of effective stresses, $\tilde{\mathbf{C}}$ is the soil damping matrix as a function of the mass and stiffness matrices ($\tilde{\mathbf{C}} = \delta\,\tilde{\mathbf{M}} + \beta\,\tilde{\mathbf{K}}$, where δ and β are the Rayleigh coefficients), and $\bar{\mathbf{f}}_s$ and $\bar{\mathbf{f}}_w$ are the vectors of nodal forces associated with the solid and water phases. For convenience, Equation 6 can be represented as

$$\mathbf{M}\bar{\mathbf{a}} + \mathbf{C}\bar{\mathbf{v}} + \mathbf{K}\bar{\mathbf{d}} = \bar{\mathbf{f}} \tag{7}$$

where **M**, **C** and **K** are generalised mass, damping and stiffness matrices, respectively, $\bar{\mathbf{f}}$ is the nodal force vector, and $\bar{\mathbf{a}} = [\ddot{\mathbf{u}}, \ddot{\mathbf{p}}]^T$, $\bar{\mathbf{v}} = [\dot{\mathbf{u}}, \dot{\mathbf{p}}]^T$, and $\bar{\mathbf{u}} = [\mathbf{u}, \mathbf{p}]^T$ are the generalised nodal acceleration, velocity, and displacement fields, respectively. By using Newmark's (1959) time integration technique, Equation 7 can be transformed into its implicit time incremental form as given by Equations 8 and 9:

$$\hat{\mathbf{K}}^t \Delta\bar{\mathbf{u}}^k = \bar{\mathbf{f}}^t - \mathbf{M}^t\left(\frac{4\Delta\bar{\mathbf{u}}^{k-1}}{\Delta t^2} - \frac{4\bar{\mathbf{v}}^t}{\Delta t} - \bar{\mathbf{a}}^t\right) - \mathbf{C}^t\left(\frac{2\Delta\bar{\mathbf{u}}^{k-1}}{\Delta t} - \bar{\mathbf{v}}^t\right) \tag{8}$$

$$\hat{\mathbf{K}}^t = \mathbf{K}^t + \frac{4}{\Delta t^2}\mathbf{M}^t + \frac{2}{\Delta t}\mathbf{C}^t \tag{9}$$

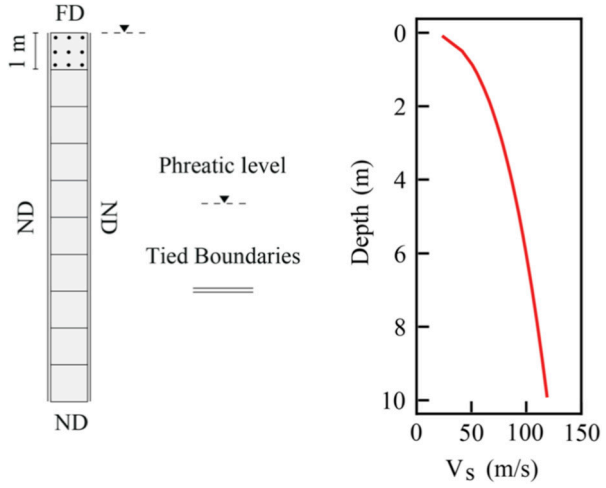

FIGURE 3
Dynamic and hydraulic boundary conditions, and shear wave velocity profile.

2.2.3 Constitutive behaviour

The hypoplastic model for granular materials (Gudehus, 1996), and its updated cyclic version (Niemunis and Herle, 1997), is a model that has been tested on multiple occasions for cyclic behaviour (Reyes et al., 2009). It has been shown to provide adequate constitutive responses under cyclic loading, such as stiffness degradation and hysteretic behaviour, and results are comparable with other recognised models (e.g., SANISAND (Dafalias and Manzari,

10.3389/fbuil.2026.1745681

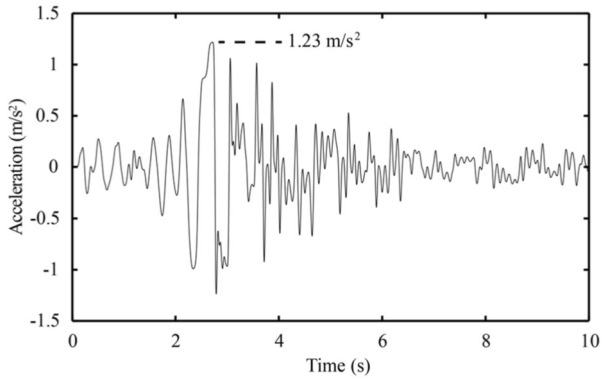

FIGURE 4
Ground acceleration of the deterministic 1D column.

2004), UBCSAND (Beaty and Byrne, 1998)) as demonstrated in comparative studies and applications reported by Wichtmann et al. (2019) and Giridharan et al. (2020). Hence, it is considered an appropriate model for the present study.

Hypoplasticity is a model in which the soil state can be adequately described by the stress state and the void ratio. The general form of the hypoplastic equation is given by Equation 10:

$$\dot{\boldsymbol{\sigma}} = \mathbf{L}: \dot{\boldsymbol{\varepsilon}} + \mathbf{N}\|\dot{\boldsymbol{\varepsilon}}\| = \boldsymbol{Z}: \dot{\boldsymbol{\varepsilon}} \tag{10}$$

where $\dot{\boldsymbol{\sigma}}$ is the Jaumann objective stress rate, $\dot{\boldsymbol{\varepsilon}}$ is the strain rate, $\mathbf{L}$ and $\mathbf{N}$ are the constitutive tensors depending on the stress and void ratio, and $\boldsymbol{Z}$ denotes the tangent stiffness of the model ($\mathbf{D}$ in Equation 5). The yield surface in the hypoplastic model is given by von Wolffersdorff (1996) as shown in Equation 11:

$$Y = \sqrt{\frac{\tan^2\psi}{8} + \frac{2-\tan^2\psi}{2+\sqrt{2}\tan\psi\cos 3\boldsymbol{\theta}}} - \frac{\tan\psi}{2\sqrt{2}} \tag{11}$$

where the stress invariants are defined in Equation 12 as

$$\hat{\boldsymbol{\sigma}} = \frac{\boldsymbol{\sigma}}{tr(\boldsymbol{\sigma})}; \hat{\boldsymbol{\sigma}}_d = \hat{\boldsymbol{\sigma}} - \frac{1}{3}\mathbf{I}; \cos 3\boldsymbol{\theta} = \frac{-\sqrt{6}\,tr(\hat{\boldsymbol{\sigma}}_d \cdot \hat{\boldsymbol{\sigma}}_d \cdot \hat{\boldsymbol{\sigma}}_d)}{(\hat{\boldsymbol{\sigma}}_d : \hat{\boldsymbol{\sigma}}_d)^{3/2}}; \tan\psi = \sqrt{3}\|\hat{\boldsymbol{\sigma}}_d\| \tag{12}$$

where $\mathbf{I}$ is an identity tensor. To account for cyclic behaviour, the "Intergranular Strain" concept has been included, where the tangential stiffness $\boldsymbol{Z}$ can be expressed as a function of $\mathbf{L}$ and $\mathbf{N}$ as given in Equation 13:

$$\boldsymbol{Z} = [\xi^{\chi} m_T + (1-\xi^{\chi}) m_R]\mathbf{L} + \begin{cases} \xi^{\chi}(1-m_T)\mathbf{L}: \hat{\mathbf{h}} \otimes \hat{\mathbf{h}} + \xi^{\chi}\mathbf{N} \otimes \hat{\mathbf{h}} & \text{for } \hat{\mathbf{h}}: \dot{\boldsymbol{\varepsilon}} > 0 \\ \xi^{\chi}(m_R - m_T)\mathbf{L}: \hat{\mathbf{h}} \otimes \hat{\mathbf{h}} & \text{for } \hat{\mathbf{h}}: \dot{\boldsymbol{\varepsilon}} \le 0 \end{cases} \tag{13}$$

where m_T, m_R and χ are intergranular parameters, and $0 \le \xi \le 1$ is the normalised magnitude of the intergranular strain $\mathbf{h}$, calculated by Equation 14:

$$\xi = \frac{\|\mathbf{h}\|}{R} \tag{14}$$

where R is a constant representing the elastic range. Note that $\mathbf{h}$ evolves towards $\dot{\boldsymbol{\varepsilon}}$ and its norm towards R as given in Equation 15:

$$\dot{\mathbf{h}} = \begin{cases} \left(\mathbf{I} - \hat{\mathbf{h}} \otimes \hat{\mathbf{h}}\xi^{\beta_r}\right): \dot{\boldsymbol{\varepsilon}} & \text{for } \hat{\mathbf{h}}: \dot{\boldsymbol{\varepsilon}} > 0 \\ \dot{\boldsymbol{\varepsilon}} & \text{for } \hat{\mathbf{h}}: \dot{\boldsymbol{\varepsilon}} \le 0 \end{cases} \tag{15}$$

where β_r is another intergranular parameter controlling the intergranular strain evolution rate, and $\hat{\mathbf{h}} = \mathbf{h}/\|\mathbf{h}\|$. The reader is directed to Niemunis and Herle (1997) for further details of the adopted hypoplastic formulation.

3 Deterministic free-field ground response and liquefaction triggering

This section studies the free-field ground response and liquefaction triggering of a standard 1D soil column assuming a homogeneous material. The results obtained from this simulation are taken as the reference deterministic (D) solution for the subsequent investigation.

3.1 Ground acceleration and soil properties

To study free-field ground response, as well as liquefaction triggering and evolution, the 1999 Chi-Chi earthquake (Figure 2) with a PGA of 0.81 m/s^2 has been selected to represent the incoming base acceleration (details of the recording station are provided in the caption of Figure 2). The selection of this ground motion was based on two factors: its availability, and its potential to trigger liquefaction with respect to the soil properties, while avoiding excessively strong input motions that could result in widespread liquefaction. Since simulating the whole earthquake proved to be unnecessary, the time window between 12 s and 22 s has been selected. An additional window is added to Figure 2 indicating the initial 2 seconds of the earthquake (between 12 and 14 s of the full earthquake), to show the initialisation of the earthquake (as modelled) from an acceleration equal to 0 m/s^2. A Fourier Amplitude Spectrum analysis of the analysed earthquake acceleration input indicates that the dominant frequency range lies between 1 and 5 Hz. The soil intrinsic parameters have been chosen to depict a standard cohesionless soil stratum, since these parameters serve mainly to investigate the limitations of traditional 1D simulations in the presence of spatial variability rather than to analyse a specific site. Table 1 shows the soil parameter values used for the hypoplastic model, in which the definitions (and calibration) of the various parameters can be found in Herle and Gudehus (1999) and Mašin (2019). These parameter values were previously calibrated for Hochstetten sand, a material that has been successfully validated, both at the element and boundary value scales, to study soil liquefaction and free-field ground response (Osinov, 2000; Nagula, 2021). The saturated unit weight of the soil and the initial total and effective stresses are computed based on a specific gravity of Gs = 2.65, the mean void ratio (introduced later), and a lateral earth pressure coefficient of K_0 = 0.45 computed using K_0 = 1-sinϕ (Jaky, 1948), where $\phi = \phi_c$, the critical state friction angle. Furthermore, to induce a fully undrained behaviour, an artificially low permeability (located in the matrix $\mathbf{H}$ in Equation 6) of $k = 1.0 \times 10^{-8}$ m/s in the horizontal and vertical directions has been adopted. Regarding the Rayleigh damping coefficients, values of 0.3665 s^{-1} for δ and 0.00185 s for β have been used, giving a target damping ratio of ζ = 3.5%. Note that these damping coefficients have been computed using the target

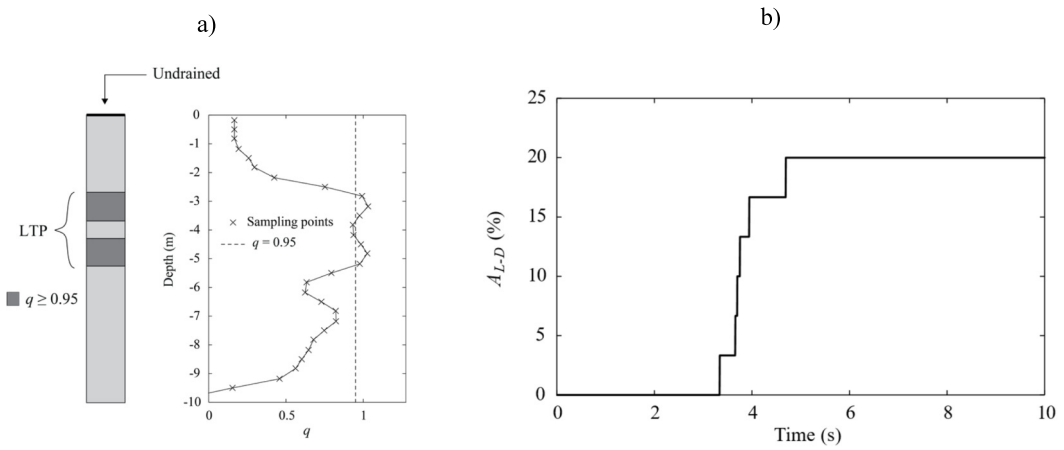

FIGURE 5
(a) Liquefied zones after the earthquake next to the variation of q with depth, and **(b)** deterministic liquefied area A_{L-D} as a function of time.

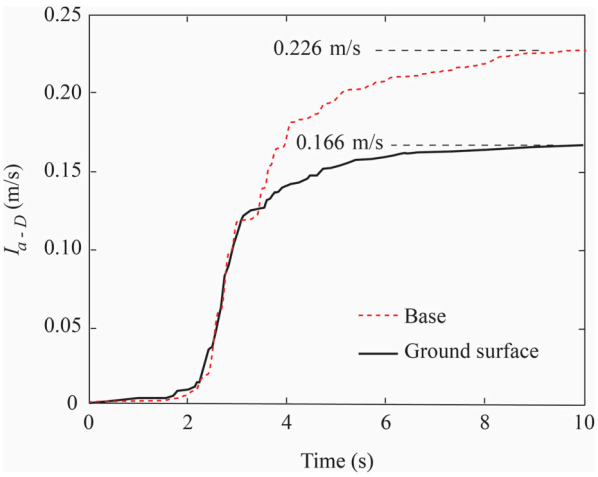

FIGURE 6
Arias intensity of deterministic solution I_{a-D}.

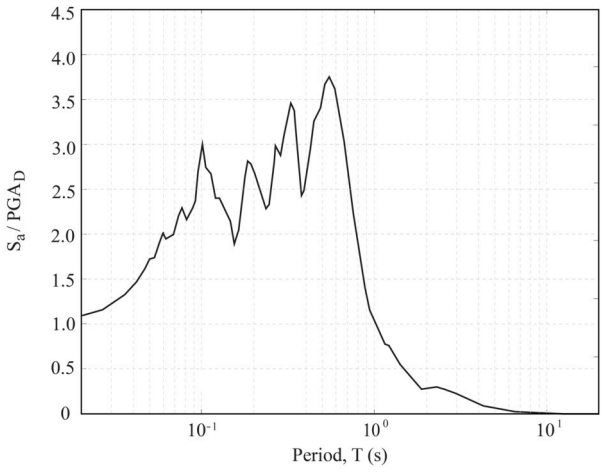

FIGURE 7
Response spectrum function of the deterministic solution (RSF_D).

frequencies of 1 Hz and 5 Hz and the classical Rayleigh damping method, as described in standard references (e.g., Chopra, 1995).

For the 1D (and later 2D) domains that have been analysed in this paper, nine node quadrilateral (plane strain) elements, of size 1 m × 1 m, with nine Gauss points per element, were used. The 1D mesh models a soil layer of 10 m thickness. The upper boundary (i.e., the soil surface) has been taken as fully drained (i.e., the pore pressures at the surface nodes are equal to zero throughout the simulation). The other boundaries have been considered impermeable. To guarantee the correct simulation of the ground seismic behaviour, periodic boundary conditions have been implemented (Cook et al., 1989), which have been observed to yield accurate results regardless of the soil spatial variability (González Acosta et al., 2023). Figure 3 depicts the dynamic and hydraulic boundary conditions, in addition to the shear velocity profile. FD and ND indicate fully drained and no drainage (impermeable), respectively, while the computed shear wave velocity (Vs.) has been obtained via the constitutive model, the *in-situ* stress state and the parameters listed in Table 1. In this case, the minimum (at the top) and maximum (at the bottom) shear wave velocities are 38.9 m/s and 117.2 m/s, respectively. Note that the minimum shear wave velocity has been used to comply with the element size recommendation given by Kuhlemeyer and Lysmer (1973), whereby the characteristic element size should be smaller than $V_{s,min}/8f_{max}$, where $V_{s,min}$ is the minimum shear wave velocity, and f_{max} is the maximum target frequency described earlier.

3.2 Deterministic solution

To analyse the free-field ground response and liquefaction triggering and evolution, the following indicators are used. Liquefaction is assessed using the liquefaction index q_i (Seed, 1979), which is numerically equivalent to the pore pressure ratio commonly denoted as r_u, and computed as $q_i = u_i/\sigma_{v,i}$, where u_i is the excess pore water pressure and $\sigma_{v,i}$ is the initial vertical effective

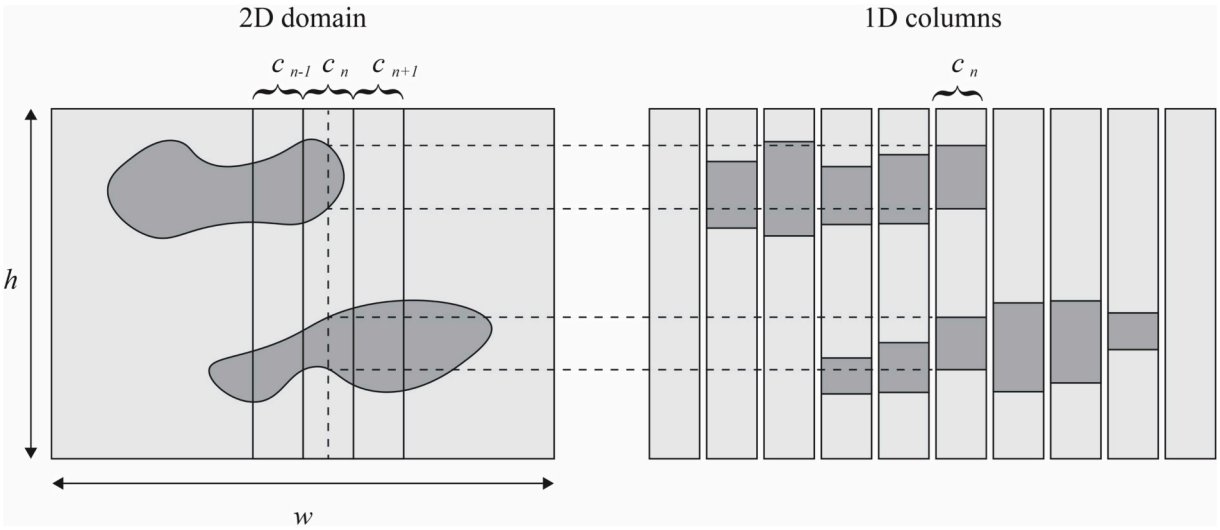

FIGURE 8
Partition of a 2D domain into 1D columns (not to scale).

stress, with all variables measured at the element Gauss point *i*. Although liquefaction is generally considered to occur when $q_i = 1$, in this paper $q_i \geq 0.95$ is accepted as a liquefied material [similar to the approach of Fenton and Vanmarcke (1998)]. The accumulated area liquefied (A_L) at any instant in time is computed using Equation 16:

$$A_L\ (\%) = \frac{\sum_{i=1}^{n_t} n_i}{n_t} \cdot 100; \quad n_i = \begin{cases} 1 & \text{for } q_i \geq 0.95 \\ 0 & \text{for } q_i < 0.95 \end{cases} \tag{16}$$

were n_t is the total number of Gauss points. For quantifying ground motion intensity, PGA values are estimated based on the largest amplitude obtained in a full surface ground motion record (i.e., the highest PGA recorded among all Gauss points adjacent to the ground surface). However, since PGA values do not consider the full duration of the earthquake, the Arias intensity (Arias, 1970) is also computed. The Arias intensity is a measure of the energy released over the full surface ground acceleration record and is computed using Equation 17:

$$I_a = \frac{\pi}{2g} \int_0^t a(t)^2\, dt \tag{17}$$

were g is the acceleration due to gravity and t is the earthquake duration. One of the advantages of I_a is that it can be used to measure the destructive potential of an earthquake (Travasarou et al., 2003). Finally, for the seismic assessment of a theoretical superficial structure, the RSF is used, representing the peak acceleration response of a range of oscillating systems subjected to the computed ground surface acceleration and computed by using a frequency-domain analysis (i.e., Fourier Transform). Figure 4 shows the computed ground surface acceleration for the deterministic (i.e., using the parameters of Table 1) 1D column subjected to the earthquake in Figure 2. It is observed that the peak acceleration is PGA_D = 1.23 m/s^2 and that it occurs at 2.7 s relative to the start of the time window.

Figure 5a shows the final stage of the (visually) undeformed deterministic solution, where the portions of soil that reached liquefaction are depicted by a darker grey colour, next to the values of q_i along the depth, and Figure 5b shows the accumulated A_L over time. From this figure, two important aspects are observed. The first is that, with 1D schemes, liquefaction triggers horizontally and instantaneously. This is evident by examining Figure 5a, where the 1D column of elements portrays perfectly horizontal liquefied layers. Furthermore, Figure 5b reinforces this notion of instantaneous horizontal liquefaction via the vertical lines which indicate full rows of Gauss points being triggered. The second aspect is the development of a liquefaction triggering position (LTP). This LTP is a function of the soil properties and the earthquake characteristics (e.g., peak acceleration, frequencies content) and indicates where the soil deposit is prone to liquefy, as has been illustrated in Figure 5a. Despite this position enclosing a certain length, not all Gauss points satisfy the $q_i \geq 0.95$ rule, which results in the appearance of two distinct portions of liquefied soil. Nonetheless, it is observed in Figure 5a that the remaining two rows of Gauss points at the centre of the LTP are near the $q_i \geq 0.95$ criterion, indicating an almost liquefied state. These results are the product of using homogeneous properties throughout the 1D column, although the presence of vertical spatial variability will also result in similar features (i.e., in terms of horizontal and instantaneous liquefaction triggering). Furthermore, it is important to remark that the liquefaction of a full row of Gauss points does not imply the full liquefaction of an element, so that seismic waves can still be transmitted vertically. Also, the final deterministic liquefied area of $A_{L\text{-}D}$ = 20.0% would be the same even were the model to be horizontally increased in size, so long as the properties remain homogeneous throughout the domain or are variable only in the vertical direction.

Figure 6 shows the Arias intensity, at the base (input earthquake) and at the ground surface, of the deterministic solution, in which the computed maximum value at the ground surface at end of the analysis is $I_{a\text{-}D}$ = 0.166 m/s. It is observed that, after 10 s, the intensity

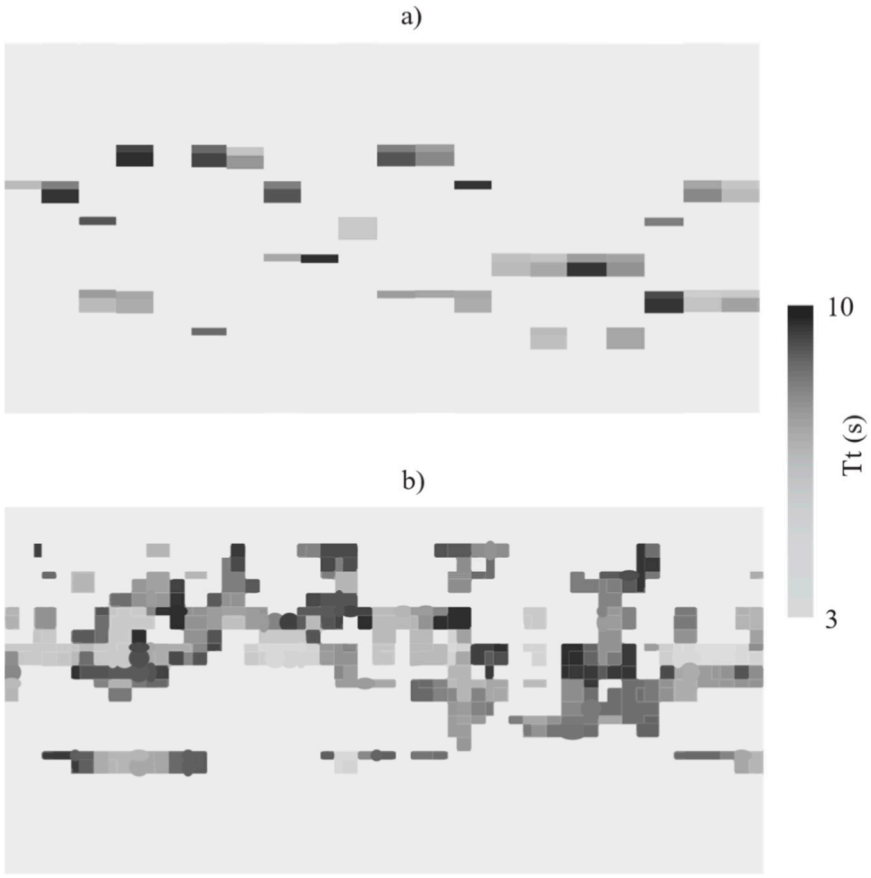

FIGURE 9
Evolution of A_L with time for **(a)** 1D columns and **(b)** 2D domain.

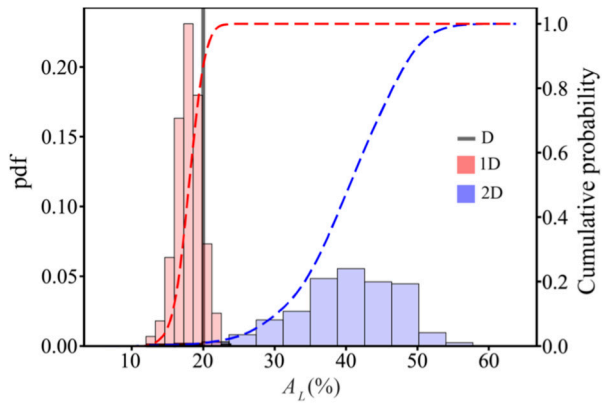

FIGURE 10
Pdf and cumulative probability of A_L reached at the end of the earthquake for 1D and 2D analyses, compared with the deterministic solution.

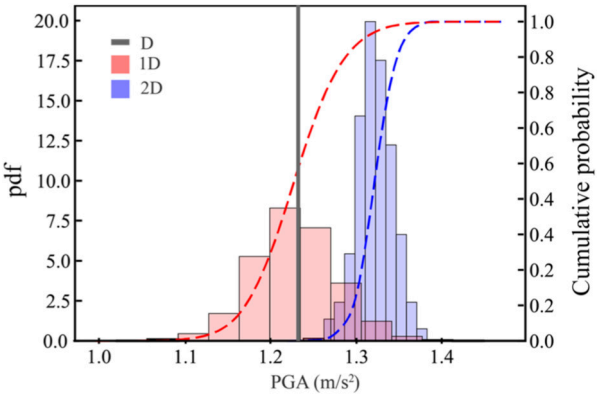

FIGURE 11
Pdf and cumulative probability of PGA values reached during the earthquake for 1D and 2D analyses, compared with the deterministic solution.

is still growing. Nevertheless, the growth can be considered as inconsequential since the earthquake, at this point, has almost ceased. The figure also shows that the base $I_{a\text{-}D}$ is larger than the corresponding ground surface $I_{a\text{-}D}$. This is because the triggering of liquefaction impedes the travelling of the seismic waves to the ground surface, thereby reducing the final ground surface energy released.

The response spectrum function of the deterministic solution RSF_D can be seen in Figure 7. This was computed using the ground acceleration data shown in Figure 4 and covers a range of oscillating

10.3389/fbuil.2026.1745681

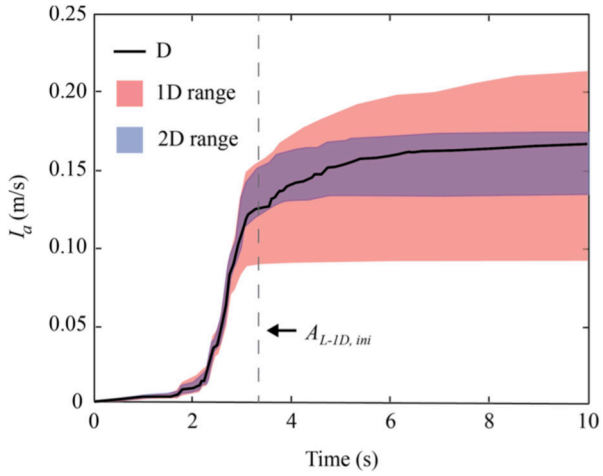

FIGURE 12
Ranges of I_a values during the earthquake.

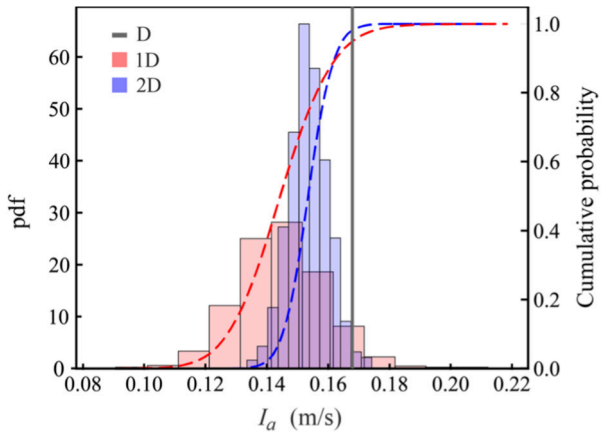

FIGURE 13
Pdf and cumulative probability of I_a values reached at the end of the earthquake for 1D and 2D analyses, compared with the deterministic solution.

single degree of freedom systems, each with a specific period T. Note that the computed spectral acceleration values (S_a) are normalized against the PGA_D. The relevance of plotting the RSF_D is to compare the deterministic solution against the results obtained from the 1D and 2D simulations considering spatial variability.

4 Assessment of traditional techniques

4.1 Problem description

To assess the limitations of traditional techniques to analyse free-field ground response and liquefaction triggering, a domain of width w = 20 m and height h = 10 m was created to perform 2D earthquake simulations considering the full spatial distribution of void ratio values (all other soil properties remain the same across all simulations). 1D simulations have also been performed, by constructing 1D columns using the corresponding material distribution of the 2D domain divided into n columns (c), hence guaranteeing the equivalence between the 1D and 2D simulations. The 1D columns extracted from the two-dimensional domains have a width equal to the element size (i.e., 1 m). Figure 8 shows a representation of the 2D domain and its partition into 1D columns. From this example, it is observed that: (1) the properties of each 1D column match perfectly the properties at the centre of each column c of the 2D domain, and (2) the properties in each 1D column extend over the width of the column, a procedure followed in traditional site response analysis. Note that, despite the group of 1D columns in Figure 8 being next to each other, the simulation of each column is independent; thus, there is no horizontal interaction between columns.

Regarding the void ratio stochastic attributes, a mean value of e_μ = 0.75, corresponding to a relative density of D_r = 50%, has been selected. (Note that, in Table 1, e_{d0} and e_{c0} correspond to the minimum and maximum void ratio, respectively.) Furthermore, based on numerous laboratory and field tests on sandy materials (Lancellotta, 1983; Lacasse and Nadim, 1996; Deodatis et al., 2014), a standard deviation of e_σ = 0.04 has been considered, corresponding to the minimum expected standard deviation for this quantity in the field. Assuming a normal distribution, it is expected that the lower and upper boundaries of the void ratio values are approximately given by $e_\mu \pm 3e_\sigma$ (i.e., $0.63 \le e \le 0.87$), suggesting that the expected relative densities encountered in the domain will be within the range $0.2 \le D_r \le 0.8$, an important detail that will justify certain results of the 1D simulations. Finally, scales of fluctuation of θ_H = 5.0 m and θ_V = 1.0 m are considered. These parameters were selected to facilitate the study of liquefaction and soil spatial variability, noting that no universally accepted values exist for their definition.

4.2 Results

In the following investigation, the results of a Monte Carlo simulation involving 1,200 realisations are shown. This number of realisations was found to be ample for achieving convergence of the output response (i.e., no further variation of the output statistics). For each 2D realisation, 20 1D analyses were performed, corresponding to the partition of the 20 m wide domain into 20 one-dimensional columns. For the presentation of the results, the liquefaction area (A_L) reported for the 1D simulations was obtained by averaging the results of the 20 1D columns. In contrast, the presented PGA, I_a and response spectra results are those computed from the individual 1D simulations.

Figure 9 shows a comparison between 1D and 2D results, for a single realisation (a single sample) of the Monte Carlo simulation, in terms of the increase in A_L with liquefaction triggering time (Tt). Figure 9a shows the results of the 1D columns, corresponding to the material properties of the 2D domain in Figure 9b. As observed, despite both domains having equivalent properties (considering the partition explained in Figure 8), the evolution of A_L is very different for the two cases. Since the 1D columns are not connected, the progressive increase in A_L results from a collection of isolated (liquefied) spots rather than from the spread of liquefaction. Furthermore, the A_L spots and triggering times of the 1D columns do not generally coincide with the 2D results, and the

10.3389/fbuil.2026.1745681

TABLE 2 Results for the distributions show in Figures 10, 11, 13.

Figures	Variable	D	Results					
			1D			2D		
			Mean	Range	CV (%)	Mean	Range	CV (%)
10	A_L (%)	20.0	18.0	12.0–23.8	29.9	40.0	12.2–57.7	17.7
11	PGA (m/s^2)	1.23	1.23	1.05–1.44	3.56	1.32	1.23–1.38	1.81
13	I_a (m/s)	0.166	0.144	0.090–0.212	9.58	0.153	0.133–0.174	4.18

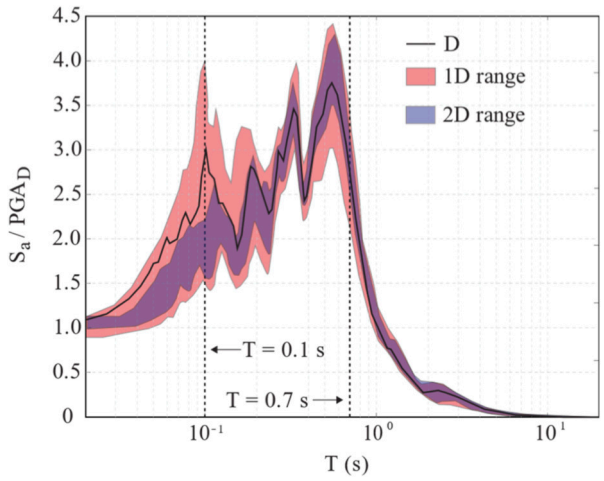

FIGURE 14
Ranges of response spectra for 1D and 2D realisations, compared with the deterministic solution.

rate of increase of A_L is considerably smaller in the 1D case than in the 2D case.

Figure 10 shows the pdf of A_L and its cumulative probability reached at the end of each realisation, for both 1D and 2D simulations. For the 1D results, each group of 20 1D columns per each 2D domain was averaged to obtain the A_L estimation, thereby accounting for the same soil random field as the 2D simulation. It is observed that the 1D and 2D distributions are located far from each other. While 2D schemes allow liquefaction spreading in all directions, which consistently results in A_L reaching values above A_L = 20%, 1D schemes impede it and stop it altogether in the horizontal plane, thereby reducing the overall A_L reached. Hence, it is clear from this set of results that 1D schemes return highly unlikely scenarios (with the computed A_L typically being well below half the 2D A_L), which is a consequence of reducing the free-field response analysis to uncoupled 1D columns. It is also seen that the deterministic solution based on the mean void ratio represents a lower bound to the 2D results, while being greater than the mean of the 1D results.

Figure 11 shows the pdf's and cumulative probability of PGA values obtained during each realisation. In this figure, the deterministic solution is located close to the mean value of the 1D results and is a lower bound to the 2D results. It is also seen that the 1D distribution is 2.6 times wider than the 2D distribution (albeit with a lower mean). The main reason for this difference is that, due to the isolation of each 1D column, the horizontal interaction of portions of soil with high and low values of e is non-existent, permitting 1D simulations to reach extreme (high and low) PGA values and thereby causing the wider distribution. On the other hand, the horizontal interaction of high and low values of e in 2D simulations causes an averaging effect within simulations, thereby resulting in a narrower distribution.

Figures 12, 13 show the ranges and pdf plots of I_a values obtained during and at the end of the earthquake, respectively. In these figures it is observed that the range of 2D results is enclosed by the wider range of 1D results, but with the 2D analyses tending to predict the greater energy released (Figure 13). In Figure 12, it is interesting to highlight that, in both the 1D and 2D cases, the rate of increase of I_a starts to reduce near the time when $A_{L\text{-}D}$ starts increasing ($A_{L\text{-}1D,\ ini} \approx 3.34$ s), which is a strong indication that this reduction in the increase of I_a is associated with the start of liquefaction. Figure 13 shows that the pdf's of I_a have mean values well below the deterministic solution. This indicates that, in the absence of weak spots of loose sand (i.e., high e values), the homogeneous 1D column produces stronger responses that tend towards the upper bound solution.

Table 2 summarises the results of the distributions shown in Figures 10, 11, 13. From the computed coefficients of variation (CV), it is observed that the variability of the 1D results is higher than that of the 2D results relative to their respective means. Finally, Figure 14 shows the ranges of the RSF's for the 1D and 2D simulations. The findings in Figure 14 are consistent with the results shown in Figures 11, 13, where the wider distribution of 1D results encompasses the range of 2D results. Furthermore, after analysing Figure 14, a clear difference is observed either side of T = 0.7 s. Above T = 0.7 s, the 1D, 2D and deterministic solutions are similar, indicating that soil spatial variability and 1D and 2D schemes do not affect the ground response when the earthquake acceleration is constituted of cycles with large periods. Note that, in the presence of large periods, the soil structure does not suffer a strong deterioration, resulting in similar results independent of the inclusion of spatial variability or the use of 1D or 2D schemes. In contrast, below T = 0.7 s, the difference between the solutions is perceptible, indicating that, for shorter periods, the effects of soil spatial variability and the use of 1D or 2D schemes can have a big influence on the outcome due to the significant degradation of the soil structure caused by the cyclic loading. It is observed that the upper boundary of the 2D results lies mostly below the deterministic and 1D solutions, especially for lower values of T, suggesting that traditional 1D methods will generally produce over-conservative RSF responses.

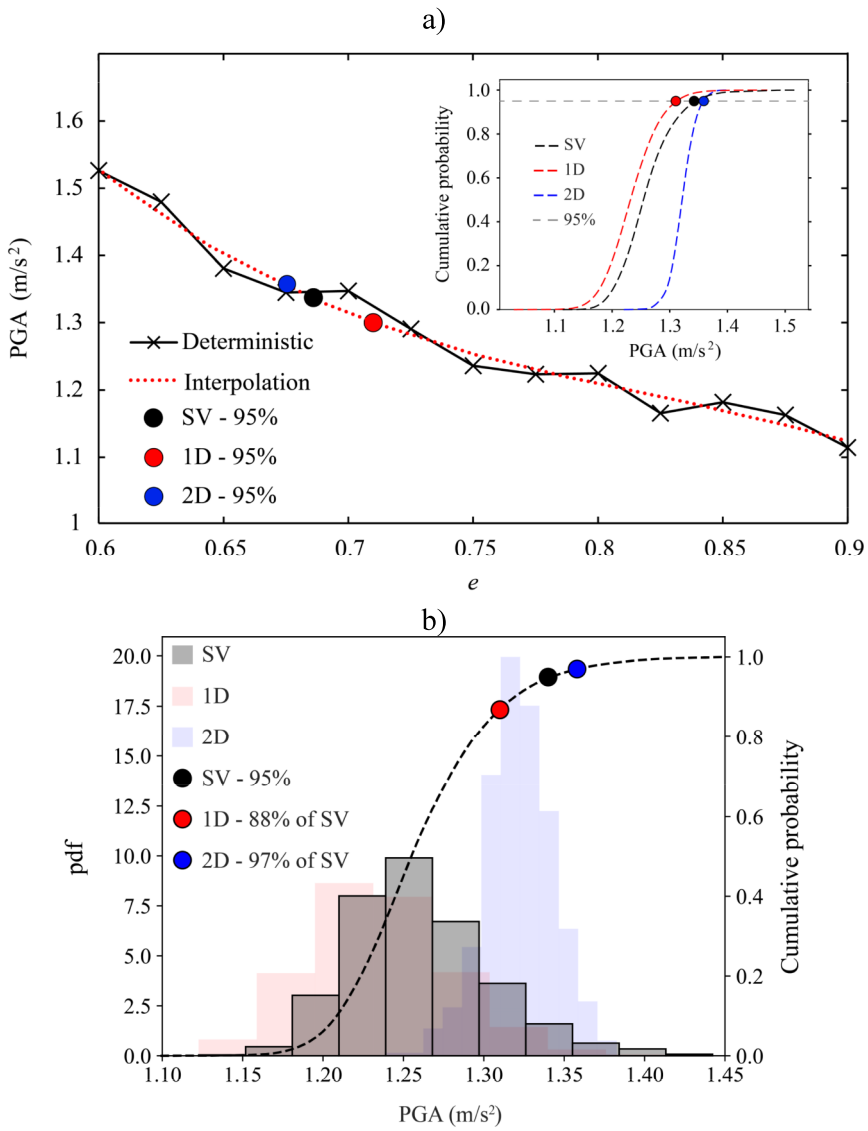

FIGURE 15
(a) PGA values as a function of *e* and the reliability levels of 95% for the SV, 1D and 2D solutions, and **(b)** locations of the 95% characteristic values with respect to the SV distribution based on the normal distribution of *e*.

Furthermore, the range of 1D results is larger than the range of 2D results at shorter periods; in this case, a peak difference occurs at T = 0.1 s, where the range of results in the 1D simulations is approximately 3.8 times larger than in the 2D simulations.

4.3 Characteristic values

In geotechnical engineering, characteristic values are conservative values used to account for uncertainties and variations in soil properties. Some authors have proposed approaches to compute characteristic values for a diverse range of geotechnical structures (Orr, 2017; Hicks et al., 2019; Varkey et al., 2020), in order to find those properties that will ensure a factor of safety that corresponds to a desired level of reliability. Based on the results presented in Section 4.2, PGA values are here examined to derive the characteristic value of *e* in terms of ground motion amplitude. Since *e* is the main stochastic parameter, a family of deterministic solutions has been computed by using different values of *e*. Figure 15a shows the series of deterministic results as a function of *e*, as well as the third order interpolation of the deterministic outcomes in terms of PGA. Figure 15a also shows the values of *e* corresponding to a reliability level of 95% for PGA distributions computed from Monte Carlo simulations involving single variables (SV) of *e*, and from the 1D and the 2D RFEM analyses, as well as the respective cumulative probability functions. Also, it should be noted that (i) the pdf and cumulative distribution function of PGA computed using the SV approach, shown in Figure 15b, have been obtained by sampling directly from the normal distribution of *e* and using the third order function in Figure 15a (i.e., without accounting for the spatial variability within realisations as in an RFEM analysis), (ii) the deterministic PGA versus *e* relationship is used to map SV, 1D, and 2D RFEM probabilistic results to

10.3389/fbuil.2026.1745681

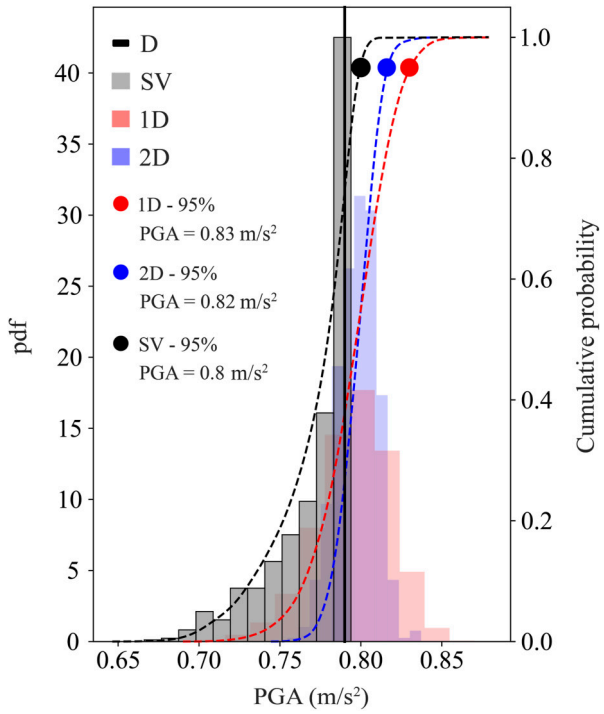

FIGURE 16
Pdf's and cumulative probabilities of PGA results considering one-quarter of the original earthquake magnitude.

corresponding values of void ratio, and (iii) although PGA alone does not fully characterise liquefaction potential, it is adopted here to maintain consistency with the preceding sections, to isolate the influence of spatial variability on the response, and because it is still a commonly used intensity measure in earthquake-related problems. Figure 15b indicates the locations of the 95–percentile characteristic values of e, as computed in the 1D and 2D RFEM simulations, relative to the SV results (as indicated in the figure legend). The relative positions suggest that the SV and 1D schemes return an under-conservative approximation (i.e., lower PGA values) compared to the more realistic 2D simulation. It is interesting to note that the 95% reliability result from the 2D simulations corresponds to the result obtained using the 97-percentile of the void ratio distribution, implying that a characteristic void ratio given by $e_\mu - 2e_\sigma$ may be appropriate for problems in which liquefaction may be possible. However, this observation is specific to the analysed input motion and modelling assumptions and is not intended as a generalised criterion for liquefaction assessment.

4.4 Low amplitude and no liquefaction conditions

For comparative purposes, the trend in results for a case in which no liquefaction occurs has also been studied. This has been achieved by repeating the previous simulations alongside a reduction in the base earthquake amplitude to one-quarter of its original value. Figure 16 shows the pdf and cumulative distribution of PGA values for the 2D domain, as well as the respective results for 1D columns and using the SV approach. Note that, in this instance, the SV results are based on the deterministic relationship between PGA values and e in Figure 17. In contrast to the previous results in Section 4.3 (based on the original earthquake), the mean values of the 1D, 2D and SV distributions are now located close to each other,

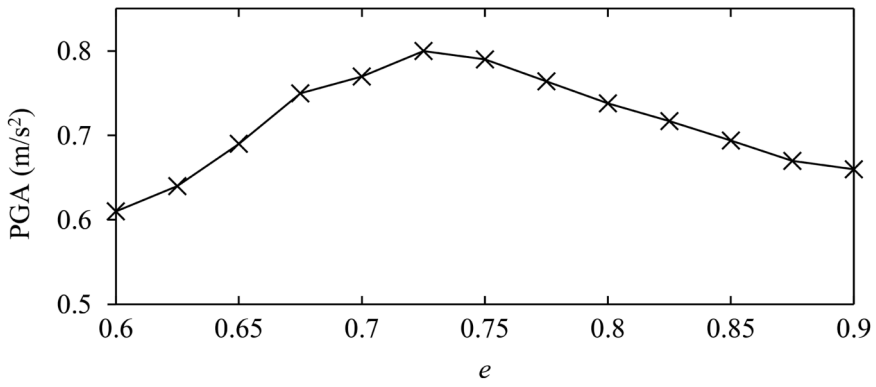

FIGURE 17
PGA deterministic results as a function of e.

TABLE 3 Results for the distributions shown in Figure 16.

Variable	Results						
	D	1D		2D		SV	
		Mean	CV (%)	Mean	CV (%)	Mean	CV (%)
PGA (m/s²)	0.79	0.795	2.88	0.797	1.5	0.771	3.25

as summarised in Table 3. However, although the differences in the mean values may be considered inconsequential, the deterministic solution does not give any indication of the uncertainty, although the 1D and 2D distributions are relatively narrow and yield smaller CV values compared to those from Table 2. These results suggest that, at lower earthquake amplitudes associated with no liquefaction, the relative difference between 1D and 2D solutions may be less significant, as has been reported in other studies (González Acosta et al., 2022b). However, a further benefit of 2D simulations, not covered in this paper, is that they provide predictions of differential settlements arising from dissipation of excess pore pressures [as described in Basu et al. (2019a) and Basu et al. (2019b)].

5 Conclusions

The reliability of traditional techniques to assess the free-field dynamic response and liquefaction potential of soil deposits has been investigated via the random finite element method for one- and two-dimensional domains by considering equivalent void ratio spatial distributions and liquefaction occurrence. In the presence of liquefaction, it was observed that, with respect to PGA, I_a, and spectral peak values, 1D schemes exhibit a larger variability of results compared to 2D simulations. This significant difference results from the greater spatial averaging in a two-dimensional framework, leading to a reduction in uncertainty. Regarding the liquefaction extent (A_L), it is difficult (if not impossible) to obtain realistic values through 1D schemes due to liquefaction spreading being prevented in the horizontal direction and hindered vertically. On the other hand, 2D schemes allow liquefaction to spread both vertically and horizontally, thereby reaching values of liquefaction extent significantly higher than those from 1D simulations. Although not analysed in this paper, it is inferred that these differences between 1D and 2D liquefaction response would significantly influence computed long-term settlements. Regarding the computed characteristic value results, it was observed that 1D techniques may return under- or over-conservative values compared to 2D schemes due to the large distribution of results. However, when the intensity of the input earthquake decreases and no liquefaction is observed, the difference between 1D and 2D simulations also decreases. As a result, 2D schemes, including spatial variability, become less influential in computing ground free-field response when the earthquake intensity is small.

Data availability statement

The raw data supporting the conclusions of this article will be made available by the authors, without undue reservation.

Author contributions

JG: Conceptualization, Formal Analysis, Investigation, Methodology, Validation, Visualization, Writing – original draft. AE: Supervision, Writing – review and editing. MH: Funding acquisition, Project administration, Supervision, Writing – review and editing.

Funding

The author(s) declared that financial support was received for this work and/or its publication. We have acknowledged the funding sources in the paper, as follows: The results presented in the paper are part of the research programme DeepNL/SOFTTOP with project number DEEP.NL.2018.006, financed by the Netherlands Organisation for Scientific Research (NWO), and was carried out on the Dutch National e-infrastructure with the support of SURF Foundation.

Conflict of interest

The author(s) declared that this work was conducted in the absence of any commercial or financial relationships that could be construed as a potential conflict of interest.

Generative AI statement

The author(s) declared that generative AI was not used in the creation of this manuscript.

Any alternative text (alt text) provided alongside figures in this article has been generated by Frontiers with the support of artificial intelligence and reasonable efforts have been made to ensure accuracy, including review by the authors wherever possible. If you identify any issues, please contact us.

Publisher's note

References

Arias, A. (1970). *A measure of earthquake intensity*. Cambridge: MIT Press.

Assimaki, D., Pecker, A., Popescu, R., and Prevost, J. (2003). Effects of spatial variability of soil properties on surface ground motion. *J. Earthq. Eng.* 7, 1–44. doi:10.1080/13632460309350472

Basu, D., Montgomery, J., and Stuedlein, A. W. (2019a). "Comparison of post-liquefaction settlements at a liquefaction test site considering numerical and empirical methods," in *Proceedings of the 7th international conference on earthquake geotechnical engineering, Rome, June 2019.*

Basu, D., Montgomery, J., and Stuedlein, A. W. (2019b). "Liquefaction-induced settlement estimates for a spatially variable deposit using numerical and empirical approaches," in *Proceedings of the 7th international symposium on geotechnical safety and risk, Taipei, December 2019.*

Beaty, M., and Byrne, P. M. (1998). "An effective stress model for predicting liquefaction behaviour of sand," in *Proceedings of geotechnical earthquake engineering and soil dynamics III, Seattle, August 1998.*

Bong, T., and Stuedlein, A. W. (2018). Effect of cone penetration conditioning on random field model parameters and impact of spatial variability on liquefaction-induced differential settlements. *J. Geotechnical Geoenvironmental Eng.* 144 (5), 04018018. doi:10.1061/(ASCE)GT.1943-5606.0001863

California Geological Survey and U.S. Geological Survey (2025). Center for engineering strong motion data (CESMD). U.S. Geological Survey. doi:10.5066/P13HTZQS

Chen, Q., Wang, C., and Juang, C. H. (2016). CPT-Based evaluation of liquefaction potential accounting for soil spatial variability at multiple scales. *J. Geotechnical Geoenvironmental Eng.* 142 (2), 04015077. doi:10.1061/(ASCE)GT.1943-5606.0001402

Chian, S. C., Tokimatsu, K., and Madabhushi, S. P. G. (2014). Soil liquefaction–induced uplift of underground structures: physical and numerical modeling. *J. Geotechnical Geoenvironmental Eng.* 140 (10), 04014057. doi:10.1061/(ASCE)GT.1943-5606.0001159

Chopra, A. K. (1995). *Dynamics of structures: theory and applications to earthquake engineering*. New Jersey: Prentice Hall.

Cook, R. D., Malkus, D. S., and Plesha, M. E. (1989). *Concepts and applications of finite element analysis*. New York: John Wiley and Sons.

Dafalias, Y. F., and Manzari, M. T. (2004). Simple plasticity sand model accounting for fabric change effects. *J. Eng. Mech.* 130 (6), 622–634. doi:10.1061/(ASCE)0733-9399(2004)130:6(622)

Deodatis, G., Ellingwood, B. R., and Frangopol, D. M. (2014). *Safety, reliability, risk and life-cycle performance of structures and infrastructures*. New York: CRC Press.

Deutsch, C. V., and Journel, A. G. (1992). *GSLIB: geostatistical software library and user's guide*. New York: Oxford University Press.

Fenton, G. A., and Griffiths, D. V. (2008). *Risk assessment in geotechnical engineering*. New York: John Wiley and Sons.

Fenton, G. A., and Vanmarcke, E. H. (1990). Simulation of random fields *via* local average subdivision. *J. Eng. Mech.* 116 (8), 1733–1749. doi:10.1061/(ASCE)0733-9399(1990)116:8(1733)

Fenton, G. A., and Vanmarcke, E. H. (1998). Spatial variation in liquefaction risk. *Géotechnique* 48 (6), 819–831. doi:10.1680/geot.1998.48.6.819

Ghaboussi, J., and Dikmen, S. U. (1977). LASS-II, computer program for analysis of seismic response and liquefaction of horizontally layered saturated sands. *Report no. UILU-ENG-77-2010*. Urbana, United States: University of Illinois at Urbana-Champaign.

Giridharan, S., Gowda, S., Stolle, D. F., and Moormann, C. (2020). Comparison of UBCSAND and hypoplastic soil model predictions using the material point method. *Soils Found.* 60 (4), 989–1000. doi:10.1016/j.sandf.2020.06.001

González Acosta, J. L., van den Eijnden, A. P., and Hicks, M. A. (2022a). "Comparison of 1D and 2D liquefaction assessment methods considering soil spatial variability," in *Proceedings of the 8th international symposium on geotechnical safety and risk, Newcastle, December 2022*.

González Acosta, J. L., van den Eijnden, A. P., and Hicks, M. A. (2022b). "Liquefaction assessment and soil spatial variation," in *Proceedings of the 6th international conference of the international association for computer methods and advances in geomechanics, Torino, August 2022*.

González Acosta, J. L., Varkey, D., van den Eijnden, A. P., and Hicks, M. A. (2023). "Periodic random fields to perform site response and liquefaction susceptibility analysis," in *Proceedings of the 10th European conference on numerical methods in geotechnical engineering, London, June 2023*.

Griffiths, D. V., and Fenton, G. A. (2004). Probabilistic slope stability analysis by finite elements. *J. Geotechnical Geoenvironmental Eng.* 130 (5), 507–518. doi:10.1061/(ASCE)1090-0241(2004)130:5(507)

Gudehus, G. (1996). A comprehensive constitutive equation for granular materials. *Soils Found.* 36 (1), 1–12. doi:10.3208/sandf.36.1

Gudehus, G., Amorosi, A., Gens, A., Herle, I., Kolymbas, D., Mašín, D., et al. (2008). The soilmodels.info project. *Int. J. Numer. Anal. Methods Geomechanics* 32 (12), 1571–1572. doi:10.1002/nag.675

Herle, I., and Gudehus, G. (1999). Determination of parameters of a hypoplastic constitutive model from properties of grain assemblies. *Mech. Cohesive-frictional Mater.* 4 (5), 461–486.

Hicks, M. A., and Onisiphorou, C. (2005). Stochastic evaluation of static liquefaction in a predominantly dilative sand fill. *Géotechnique* 55 (2), 123–133. doi:10.1680/geot.2005.55.2.123

Hicks, M. A., and Samy, K. (2002). Influence of heterogeneity on undrained clay slope stability. *Q. J. Eng. Geol. Hydrogeology* 35 (1), 41–49. doi:10.1144/qjegh.35.1.41

Hicks, M. A., Varkey, D., van den Eijnden, A. P., de Gast, T., and Vardon, P. J. (2019). On characteristic values and the reliability-based assessment of dykes. *Georisk Assess. Manag. Risk Eng. Syst. Geohazards* 13 (4), 313–319. doi:10.1080/17499518.2019.1652918

Jaky, J. (1948). "Pressure in soils," in *Proceedings of the 2nd international conference on soil mechanics and foundations engineering, Rotterdam, June 1948*.

Koutsourelakis, S., Prévost, J. H., and Deodatis, G. (2002). Risk assessment of an interacting structure–soil system due to liquefaction. *Earthq. Eng. and Struct. Dyn.* 31 (4), 851–879. doi:10.1002/eqe.125

Kuhlemeyer, R. L., and Lysmer, J. (1973). Finite element method accuracy for wave propagation problems. *J. Soil Mech. Found. Div.* 99 (5), 421–427. doi:10.1061/JSFEAQ.0001885

Lacasse, S., and Nadim, F. (1996). "Uncertainties in characterising soil properties," in *Uncertainty in the geologic environment: from theory to practice, Wisconsin, August 1996*.

Lancellotta, R. (1983). *Analisi di affidabilita in ingenieria geotecnica*. Politecnico di Torino.

Lee, K. L., and Seed, H. B. (1967). Cyclic stress conditions causing liquefaction of sand. *J. Soil Mech. Found. Div.* 93 (1), 47–70. doi:10.1061/JSFEAQ.0000945

Liu, Y., Lee, F. H., Quek, S. T., and Beer, M. (2004). Modified linear estimation method for generating multi-dimensional multi-variate Gaussian field in modelling material properties. *Probabilistic Eng. Mech.* 38, 42–53. doi:10.1016/j.probengmech.2014.09.001

Luque, R., and Bray, J. D. (2020). Dynamic soil-structure interaction analyses of two important structures affected by liquefaction during the Canterbury earthquake sequence. *Soil Dyn. Earthq. Eng.* 133, 106026. doi:10.1016/j.soildyn.2019.106026

Maharjan, M., and Takahashi, A. (2013). Centrifuge model tests on liquefaction-induced settlement and pore water migration in non-homogeneous soil deposits. *Soil Dyn. Earthq. Eng.* 55, 161–169. doi:10.1016/j.soildyn.2013.09.002

Mašin, D. (2019). *Modelling of soil behaviour with hypoplasticity: another approach to soil constitutive modelling*. Cham: Springer.

Montgomery, J., and Boulanger, R. W. (2016). Effects of spatial variability on liquefaction-induced settlement and lateral spreading. *J. Geotechnical Geoenvironmental Eng.* 143 (1), 04016086. doi:10.1061/(ASCE)GT.1943-5606.0001584

Nagula, S. S. (2021). *Optimisation of deep vibratory compaction as liquefaction mitigation measure*. Hamburg, Germany: Hamburg University of Technology. PhD Thesis.

Newmark, N. M. (1959). A method of computation for structural dynamics. *J. Eng. Mech. Div.* 85 (3), 67–94. doi:10.1061/JMCEA3.0000098

Niemunis, A., and Herle, I. (1997). Hypoplastic model for cohesionless soils with elastic strain range. *Mech. Cohesive-frictional Mater.* 2 (4), 279–299.

Orr, T. L. (2017). Defining and selecting characteristic values of geotechnical parameters for designs to Eurocode 7. *Georisk Assess. Manag. Risk Eng. Syst. Geohazards* 11 (1), 103–115. doi:10.1080/17499518.2016.1235711

Osinov, V. A. (2000). Wave-induced liquefaction of a saturated sand layer. *Continuum Mech. Thermodyn.* 12 (5), 325–339. doi:10.1007/s001610050140

Popescu, R., Prevost, J. H., and Vanmarcke, E. H. (1995). "Numerical simulations of soil liquefaction using stochastic input parameters," in *Proceedings of the 3rd international conference on recent advances in geotechnical earthquake engineering and soil dynamics, St. Louis, April 1995*.

Popescu, R., Prevost, J. H., and Deodatis, G. (1997). Effects of spatial variability on soil liquefaction: some design recommendations. *Géotechnique* 47 (5), 1019–1036. doi:10.1680/geot.1997.47.5.1019

Popescu, R., Prevost, J. H., and Deodatis, G. (2005). 3D effects in seismic liquefaction of stochastically variable soil deposits. *Géotechnique* 55 (1), 21–31. doi:10.1680/geot.2005.55.1.21

Pretell, R., Ziotopoulou, K., and Abrahamson, N. A. (2022). Conducting 1D site response analyses to capture 2D VS spatial variability effects. *Earthq. Spectra* 38 (3), 2235–2259. doi:10.1177/87552930211069400

Prevost, J. H. (1986). Effective stress analysis of seismic site response. *Int. J. Numer. Anal. Methods Geomechanics* 10 (6), 653–665. doi:10.1002/nag.1610100607

Reyes, D. K., Rodriguez-Marek, A., and Lizcano, A. (2009). A hypoplastic model for site response analysis. *Soil Dyn. Earthq. Eng.* 29 (1), 173–184. doi:10.1016/j.soildyn.2008.01.003

Seed, H. B. (1979). Soil liquefaction and cyclic mobility evaluation for level ground during earthquakes. *J. Geotechnical Eng. Div.* 105 (2), 201–255. doi:10.1061/AJGEB6.0000768

Seed, H. B., and Idriss, I. M. (1967). Analysis of soil liquefaction: Niigata earthquake. *J. Soil Mech. Found. Div.* 93 (3), 83–108. doi:10.1061/JSFEAQ.0000981

Seed, H. B., and Idriss, I. M. (1971). Simplified procedure for evaluating soil liquefaction potential. *J. Soil Mech. Found. Div.* 97 (9), 1249–1273. doi:10.1061/JSFEAQ.0001662

Seed, H. B., and Lee, K. L. (1966). Liquefaction of saturated sands during cyclic loading. *J. Soil Mech. Found. Div.* 92 (6), 105–134. doi:10.1061/JSFEAQ.0000913

Shibata, T., Yukitomo, H., and Miyoshi, M. (1972). Liquefaction process of sand during cyclic loading. *Soils Found.* 12 (1), 1–16. doi:10.3208/sandf1960.12.1

Smith, I. M., Griffiths, D. V., and Margetts, L. (2013). *Programming the finite element method*. New York: John Wiley and Sons.

Stuedlein, A. W., and Bong, T. (2017). Effect of spatial variability on static and liquefaction-induced differential settlements. in *Geo-Risk, Colo. June*, 2017. doi:10.1061/9780784480694

Sumer, B. M. (2014). *Liquefaction around marine structures*. New Jersey: World Scientific.

Travasarou, T., Bray, J. D., and Abrahamson, N. A. (2003). Empirical attenuation relationship for Arias Intensity. *Earthq. Eng. and Struct. Dyn.* 32 (7), 1133–1155. doi:10.1002/eqe.270

Vargas-Moreno, C. O., Flores, F. A., and Ortiz, R. E. (2016). *Evaluación de la vulnerabilidad a la licuación de arenas*, A.C. Ciudad de México: Sociedad Mexicana de Ingeniería Geotécnica.

Varkey, D., Hicks, M. A., and van den Eijnden, A. P. (2023). Predicting subsurface classification in 2D from cone penetration test data. *Transp. Geotech.* 43, 101128. doi:10.1016/j.trgeo.2023.101128

Varkey, D., Hicks, M. A., van den Eijnden, A. P., and Vardon, P. J. (2020). On characteristic values for calculating factors of safety for dyke stability. *Géotechnique Lett.* 10, 353–359. doi:10.1680/jgele.19.00034

von Wolffersdorff, P. A. (1996). A hypoplastic relation for granular materials with a predefined limit state surface. *Mech. Cohesive-frictional Mater. An Int. J. Exp. Model. Comput. Mater. Struct.* 1 (3), 251–271.

Wang, C., Chen, Q., Shen, M., and Juang, C. H. (2017). On the spatial variability of CPT-based geotechnical parameters for regional liquefaction evaluation. *Soil Dyn. Earthq. Eng.* 95, 153–166. doi:10.1016/j.soildyn.2017.02.001

Wichtmann, T., Fuentes, W., and Triantafyllidis, T. (2019). Inspection of three sophisticated constitutive models based on monotonic and cyclic tests on fine sand: hypoplasticity vs. Sanisand vs. ISA. *Soil Dyn. Earthq. Eng.* 124, 172–183. doi:10.1016/j.soildyn.2019.05.001

Xiao, T., Li, D. Q., Cao, Z. J., Au, S. K., and Phoon, K. K. (2016). Three-dimensional slope reliability and risk assessment using auxiliary random finite element method. *Comput. Geotechnics* 79, 146–158. doi:10.1016/j.compgeo.2016.05.024

Zienkiewicz, O. C., Chan, A. H. C., Pastor, M., Schrefler, B. A., and Shiomi, T. (1999). *Computational geomechanics with special reference to earthquake engineering*. New York: John Wiley and Sons.